Superradiance in the high-gain free-electron laser

R. Bonifacio, B. W. J. McNeil, and P. Pierini
Dipartimento di Fisica, Università di Milano, Via Celoria 16, 20133 Milano, Italy
(Received 15 December 1988)

In this paper we describe the effects of slippage on the single-pass high-gain free-electron laser (FEL) amplifier. We use a one-dimensional computational code to show the existence of two new dynamical regimes characterized by a dimensionless parameter K, which is a measure of the slippage in one gain length. We define the long-pulse limit to be when $K \ll 1$ or the electron pulse length L_e is much greater than a properly defined "cooperation length" L_c ($L_e \gg L_c$). In this case we find that only the leading region of the propagating radiation pulse exhibits the usual steady-state behavior, with peak power proportional to $n_e^{4/3}$ (where n_e is the electron-beam density). The trailing (slippage) region exhibits a spiking behavior with peak intensities reaching many times the saturated intensity predicted by steady-state theory. We define the short-pulse regime to be when $K \gtrsim 1$ ($L_e \lesssim L_c$). In this regime the peak power emitted by the electrons does not scale as $n_e^{4/3}$, as predicted by steady-state theory, but scales as n_e^2, which is typical of superradiant behavior. Furthermore, energy is extracted from the electrons in a continuous way, with no steady-state synchrotron oscillatory-type behavior.

I. INTRODUCTION

In this paper we numerically investigate pulse propagation in a single-pass high-gain free-electron laser (FEL) amplifier.[1-6] Most previous theories for the single-pass amplifier assume an infinitely long uniform density electron beam, so that one section of the electron beam (and hence radiation) evolves identically with all other sections as it passes through the amplifier (see Ref. 2 and references therein). Thus one representative section (one ponderomotive well or "bucket") of the electron and radiation beams need to be modeled to describe the interaction of the whole. Hence the relative slippage of the radiation envelope through the electrons (the radiation velocity being greater than that of the electrons) is neglected. This is known as the "steady-state" regime of the FEL amplifier. In this regime the radiation intensity emitted by the electron beam scales as $n_e^{4/3}$, where n_e is the electron-beam density.[1-3]

When pulse effects are included in a model, the relative slippage of the radiation envelope (the radiation pulse) through the electron pulse becomes important as, in general, no two sections of the electron and radiation pulses will evolve identically. Thus many sections throughout the width of the pulses need to be modeled.

In previous simulations which have included pulse effects (e.g., Ref. 7) the criterion used to describe the length of the electron pulse was the relative slippage distance between the electron and radiation pulses on passing through the FEL amplifier. An electron pulse was described as being "long" or "short" with respect to this distance. When modeling long pulses in these simulations, the evolution of the electrons and radiation in the leading and trailing regions of the pulses was ignored by use of the "wrapped-window approximation."

Pulse propagation simulation is carried out here by a computer code which models the electron and radiation pulses by a one-dimensional (1D) distribution of radiation and electron-beam parameters. This code enables the slippage of the radiation through the electron pulse to be modeled effectively for a wide range of electron pulse widths.

We redefine the electron pulse to be long or short with respect to a properly defined "cooperation length,"[8,9] this nomenclature being equivalent to that used in describing cooperative processes in atomic systems.[10]

We also allow the electron and radiation pulses to evolve over their entire lengths, permitting an examination of the radiation and electron evolution in the leading and trailing (slippage) regions of the pulses. These regions of pulse evolution has not been investigated before (to the authors knowledge).

Our model also enables further investigation of the superradiant regime of the single-pass FEL predicted in Refs. 8 and 9, where it was suggested that, if electron pulses were sufficiently short, the emitted radiation would quickly "escape" the electron pulse due to slippage. This escape of radiation would inhibit any steady-state-type saturation process. This effect was modeled phenomenologically by the introduction of a loss term in the steady-state equations governing the radiation evolution,[8,9] and it was shown that the radiation intensity now scaled as n_e^2, which is definitory of superradiant-type processes.[10]

Radiation intensities scaling as n_e^2 may also arise from coherent synchrotron radiation emitted by electrons which have been *prebunched* by an external source, e.g., a strong laser field. The radiation fields emitted by these prebunched electrons sum up coherently, to give the n_e^2 scaling. This is superradiance as defined by Dicke,[11] i.e., spontaneous emission from a coherently prepared system. In the atomic case this phenomenon takes place in photon-echo and free-induction decay experiments.

Strictly speaking, we observe a different phenomenon. Ideally, the electrons enter the wiggler in an unprepared

state, i.e., unbunched and with no input signal, so that the intensity of the emitted radiation is initially proportional to n_e (spontaneous radiation). The electrons then begin to bunch on interacting with the spontaneous radiation and wiggler fields and evolve to emit radiation with an intensity proportional to n_e^2. This behavior is a self-organizing phenomenon, whose atomic analogy has been called superfluorescence.[10]

We will refer to "superradiance" in this latter sense, i.e., radiation intensities scaling as n_e^2 from a *self-bunched* system.

We note that even in the long-pulse limit there is always a region at the trailing edge of the electron pulse which will evolve as a short electron pulse. This region occurs because there is no radiation entering from behind and all emitted radiation propagates in the forward direction. We will show that this trailing region emits superradiant radiation which, we hypothesize, is subsequently amplified on propagating through the slippage region to produce a spiking behavior with intensities much greater than the steady-state saturation value. We call this phenomenon "strong" superradiance to distinguish it from the superradiance emitted by the short electron pulses, which we call "weak" superradiance. We use the terms weak and strong superradiance as the peak intensities are smaller and greater, respectively, than those of the steady-state theory.

In Sec. II we give a brief account of the equations and computational methods used. In Sec. III we use the model to investigate long-pulse (LP) propagation; short pulses (SP) and superradiance (SR) are considered in Sec. IV. Section V gives a discussion of the spiking behavior of the radiation in the trailing region in the LP limit; a summary and a general discussion is presented in Sec. VI.

II. COMPUTATIONAL MODEL

The equations used to describe the 1D pulse evolution of the radiation and electrons are the partial differential form of the coupled Maxwell-Lorentz equations and can be written in the form of the Eqs. (1) and (2), where the usual Compton limit approximations have been made[1-5]

$$\left[\frac{\partial}{\partial z}+\frac{1}{c}\frac{\partial}{\partial t}\right]a(z,t)=\frac{4\pi e^2 n_e(z,t)}{m}\frac{a_0}{2\gamma_r c k_r}\langle e^{-i\theta(z,t)}\rangle \ , \tag{1}$$

$$\left[\frac{\partial}{\partial z}+\frac{1}{\bar{v}_\parallel}\frac{\partial}{\partial t}\right]^2\theta_m(z,t)=-\frac{k_0 k_r a_0}{\gamma_r^2}[a(z,t)e^{i\theta_m(z,t)}+\text{c.c.}], \quad m=1,\ldots,N \tag{2}$$

where $\theta_m=(k_r+k_0)z-ck_r t$ is the electron-field phase; $k_0=2\pi/\lambda_0$ is the wave number associated with the undulator periodicity λ_0; $k_r=2\pi/\lambda_r=\omega_r/c$ is the radiation wave number; $\bar{v}_\parallel=\langle\beta_\parallel\rangle c$ the average electron longitudinal velocity; $a(z,t)$ is the slowly varying complex amplitude of the dimensionless radiation vector potential $e\mathbf{A}_r/mc^2=-(i/\sqrt{2})\{\hat{\mathbf{e}}a\exp[i(k_r z-\omega_r t)]-\text{c.c.}\}$; $\hat{\mathbf{e}}\equiv\hat{\mathbf{x}}+i\hat{\mathbf{y}}/\sqrt{2}$; $n_e(z,t)$ is the electron-beam number density; and $\langle X\rangle=[1/N(z,t)]\sum_{m=1}^{N(z,t)}X_m$ is the average over the $N(z,t)$ electrons in position z at a fixed time t of the general electron variable X. The index m is used to distinguish different electrons in a beam composed of N electrons. The undulator parameter a_0 is given by $a_0=eB_w\lambda_0/2\pi mc^2$, where B_w is the magnetostatic field amplitude. Furthermore, γ_r is the resonant electron energy in units of mc^2 given by the relation $\gamma_r^2=(1+a_0^2)\lambda_0/2\lambda_r$.[1-4]

By transforming to the characteristics

$$\begin{aligned} z_1&=z-c\beta_\parallel t \ , \\ z_2&=ct-z \ , \end{aligned} \tag{3}$$

Eqs. (1) and (2) reduce to

$$(1-\beta_\parallel)\frac{\partial}{\partial z_1}a(z_1,z_2)=\frac{4\pi e^2 n_e(z_1)}{m}\frac{a_0}{2\gamma_r c k_r}\langle e^{-i\theta(z_1,z_2)}\rangle \ , \tag{4}$$

$$\frac{(1-\beta_\parallel)^2}{\beta_\parallel^2}\frac{\partial^2}{\partial z_2^2}\theta_m(z_1,z_2)=-\frac{k_0 k_r a_0}{\gamma_r^2}[a(z_1,z_2)e^{i\theta_m(z_1,z_2)}+\text{c.c.}], \quad m=1,\ldots,N \ . \tag{5}$$

Similarly to Refs. 1–3 we transform to dimensionless variables. We define

$$\begin{aligned} \bar{z}_1&=\frac{4\pi\rho}{\lambda_r\beta_\parallel}z_1=\frac{4\pi\rho}{\lambda_r\beta_\parallel}(z-c\beta_\parallel t) \ , \\ \bar{z}_2&=\frac{4\pi\rho}{\lambda_r}z_2=\frac{4\pi\rho}{\lambda_r}(ct-z) \ , \end{aligned} \tag{6}$$

where

$$\rho=\frac{1}{\gamma_r}\left[\frac{a_0}{4}\frac{\omega_p\lambda_0}{2\pi c}\right]^{2/3} \tag{7}$$

is the fundamental FEL parameter,[1-3] which scales as $\bar{n}_e^{1/3}$, and ω_p is the nonrelativistic plasma frequency, defined as $(4\pi e^2\bar{n}_e/m)^{1/2}$; $\bar{n}_e$ is the peak electron density.

Note that $\bar{z}_1$ and $\bar{z}_2$ are normalized to the *cooperation length* of Refs. 8 and 9

$$L_c \equiv \frac{\lambda_r}{4\pi\rho} \tag{8}$$

and that $L_g \equiv \lambda_0/4\pi\rho$ is the "*gain length*" (the distance through the undulator such that the gain is equal to 1) in the steady-state regime.[8,9] The cooperation length may be interpreted as *the slippage distance* in one gain length, i.e.,

$$L_c = (c - v_\parallel)\frac{L_g}{v_\parallel} = \frac{\lambda_r}{4\pi\rho} ,$$

or, alternatively, L_c is a measure of the minimum distance between which electrons may interact cooperatively via the radiation field. Here, we have assumed the resonant radiation wavelength, given by

$$\lambda_r = \lambda_0 \frac{1-\beta_\parallel}{\beta_\parallel} \simeq \frac{\lambda_0}{2\gamma_r^2}(1+a_0^2) , \tag{9}$$

which implies that the slippage in a wiggler period is equal to λ_r.

Using (6), Eqs. (4) and (5) become

$$\frac{\partial}{\partial \bar{z}_1} A(\bar{z}_1,\bar{z}_2) = f(\bar{z}_1)\langle e^{-i\theta(\bar{z}_1,\bar{z}_2)}\rangle , \tag{10}$$

$$\frac{\partial^2}{\partial \bar{z}_2^2}\theta_m(\bar{z}_1,\bar{z}_2) = -[A(\bar{z}_1,\bar{z}_2)e^{i\theta_m(\bar{z}_1,\bar{z}_2)} + \text{c.c.}] ,$$

$$m = 1,\ldots,N . \tag{11}$$

Here, $f(\bar{z}_1)$ is the macroscopic electron density function normalized to 1 at $\bar{n}_e$, propagating with the average electron velocity $\bar{v}_\parallel$ [i.e., $n_e(z,t) = f(\bar{z}_1)\bar{n}_e$] and A is the dimensionless field amplitude[1-3] defined so that

$$|A|^2 = \frac{|E_0|^2/4\pi}{n_e\gamma_r mc^2}\frac{1}{\rho} , \tag{12}$$

where E_0 is the electric-field amplitude.

Note that $\bar{z}_1 + \bar{z}_2 = \bar{z}$, where $\bar{z} = (4\pi\rho/\lambda_0)z$ is the dimensionless distance along the wiggler, generally referred to as the (unsaturated exponential) gain parameter.[1,2] This quantity increases by $4\pi\rho$ every wiggler period, i.e.,

$$\Delta\bar{z} = \Delta(\bar{z}_1 + \bar{z}_2) = \frac{4\pi\rho}{\lambda_r}\left[\frac{1}{\beta_\parallel} - 1\right]\Delta z = \frac{4\pi\rho}{\lambda_0}\Delta z = 4\pi\rho .$$

Furthermore, $\bar{z}_1$ and $\bar{z}_2$ change by steps of $4\pi\rho$ per wiggler period along the characteristics $\bar{z}_2 = \text{const}$ and $\bar{z}_1 = \text{const}$, respectively,

$$\Delta\bar{z}_1 = \frac{4\pi\rho}{\lambda_0}\Delta z \text{ for } \bar{z}_2 = \text{const, i.e., } \Delta z = c\Delta t ,$$

$$\Delta\bar{z}_2 = \frac{4\pi\rho}{\lambda_0}\Delta z \text{ for } \bar{z}_1 = \text{const, i.e., } \Delta z = c\beta_\parallel\Delta t .$$

In particular, if $\Delta z = \lambda_0$, we have $\Delta\bar{z}_1 = \Delta\bar{z}_2 = 4\pi\rho$.

From Eq. (6) we see that, if $t = \text{const}$, then $\Delta\bar{z}_1 = \Delta\bar{z}_2 = 4\pi\rho$ also corresponds to a "static" distance of $\Delta z \simeq \lambda_r$ along the pulses. Hence the "natural" unit length in which to discretize both the electron pulse and the radiation pulse is $4\pi\rho$ (i.e., λ_r).

The equations are then integrated with step size $\Delta\bar{z}_1 = \Delta\bar{z}_2 = 4\pi\rho = \Delta\tau$ per wiggler period, repeated through N_0 wiggler periods, so that the total integration interval is $4\pi\rho N_0$, i.e., the total unsaturated gain.[1-3] Furthermore, after each integration step we let the electron pulse slip behind the radiation pulse by one wavelength λ_r ($4\pi\rho$), so that at the end the total slippage length will be $L_s = N_0\lambda_r$, as required by the resonance condition (9).

It is useful to introduce the parameters associated with pulse propagation effects in the system of dimensionless units of Refs. 1-3, 8, and 9. Let L_e be the electron pulse length and $G = 4\pi\rho N_0$ the total unsaturated gain ($G > 1$) in the steady-state limit. We define the slippage parameter S as

$$S \equiv \frac{L_s}{L_e} = \frac{N_0\lambda_r}{L_e} = \frac{N_0}{N_e}$$

(where $N_e \equiv L_e/\lambda_r$) and the superradiant parameter K as

$$K \equiv \frac{L_c}{L_e} = \frac{S}{G} = \frac{1}{4\pi\rho N_e} . \tag{13}$$

Note that K^{-1} is a measure of the gain of a photon on slipping through the unsaturated electron pulse. Also, K is equal to the slippage S in one gain length L_g (when $G = 1$ or, equivalently, $N_0 = 1/4\pi\rho$). Recall that our discussion will be confined to the high-gain situation, so that $S = GK > K$ (i.e., the slippage parameter is always greater than the superradiant parameter).

The bunching of the electrons within a potential well is measured by $b \equiv \langle \exp(-i\theta)\rangle$, so that for perfect electron bunching (same θ_m for all the electrons, $m = 1,\ldots,N$), $|b| = 1$.

III. THE LONG-PULSE LIMIT: $K \ll 1$ ($L_e \gg L_c$)

From previous theories for infinitely long electron pulses ($S = 0$), i.e., in the steady-state regime, the dimensionless intensity $|A|^2$ rises exponentially from a noise source value to a saturated value $|A|^2_{\text{sat}} \simeq 1.4$ (Refs. 1-3). It then oscillates at a frequency determined by the synchrotron period.

In this section we use the computational model, described in Sec. II, to reexamine the output from the single-pass amplifier in the long electron pulse (LP) limit.

Unlike previous theories where this regime was characterized by the slippage parameter $S \ll 1$, we will show that this regime is more correctly characterized by the more stringent condition

$$K \ll 1 \Longrightarrow L_e \gg L_c . \tag{14}$$

The opposite case, when

$$K \gtrsim 1 \Longrightarrow L_e \lesssim L_c ,$$

we characterize as the short-pulse (SP) limit.

That is, we define the electron pulse to be *long* or *short*

with respect to the cooperation length L_c (not necessarily with respect to the slippage distance $L_s = N_0\lambda_r$).

Because the redefined long-pulse regime is no longer dependent on the wiggler length $L_0 \equiv N_0\lambda_0$, we define two long-pulse subcases: The long wiggler ($S \gtrsim 1$), i.e., $N_0 \gtrsim N_e$ and the short wiggler ($S < 1$), i.e., $N_0 < N_e$.

Note that with high-gain ($G > 1$) the SP limit necessarily implies $S > 1$, i.e., the long-wiggler limit.

We now model a typical long-pulse–short-wiggler (LPSW) case.

For the purpose of investigating LPSW effects here we inject an electron pulse (say) 400 radiation wavelengths long. (This corresponds to 400 electron-pulse "strips" in the computational simulation, one strip corresponding to a discretized element of width λ_r.) The wiggler has 100 periods, so that the slippage parameter is $S = \frac{1}{4}$, with $G = 30$ and $K = \frac{1}{120}$.

We have assumed a monoenergetic square electron-density distribution on entering the wiggler, so that the function $f(\bar{z}_1) = 1$ throughout the electron pulse. We also assume resonance and so set $\partial\theta/\partial\bar{z}_2 = 0$ for all electrons. In Table I we list the parameters used in this simulation.

Computational output of the electron and radiation pulses has the following format: the radiation output intensity $|A|^2$ is plotted in a "window" traveling at velocity c at various positions through the wiggler (after N_P wiggler periods). The position within this window is given in units of λ_r from its trailing edge. The width of the window is then given by the width of the electron pulse plus the distance by which the electron pulse slips with respect to the radiation in the wiggler, i.e., $N_e + N_0$.

The average of the electron-energy detuning parameter $\langle \dot{\theta} \rangle \equiv \langle \partial\theta/\partial\bar{z}_2 \rangle = (1/\rho)\langle (\gamma - \gamma_r)/\gamma_r \rangle$, corresponding to the "energy loss per strip," is plotted in a similar type window of width N_e above the radiation pulse. Since the electrons travel at velocity $\beta_\parallel c < c$, the electron pulse window is seen to slip behind the radiation pulse window. This slippage is determined by the resonance condition and is then equal to "one strip per wiggler period." In this way both electron and radiation pulse parameters (here $\langle \dot{\theta} \rangle$ and $|A|^2$) may be plotted at various points through the wiggler. In Fig. 1 we show this series of plots as the radiation-electron pulses pass through the wiggler.

The windows of the electron-radiation pulses have their leading-edge synchronous at the start of the wiggler, not shown in the figure. The radiation window is "seeded" with a small uniform field—$|A_0|^2 = 2\times10^{-4} \ll |A|^2_{\text{sat}}$— and the electrons are uniformly distributed in pendulum phase θ with energy detuning parameter $\dot{\theta} = 0$. This allows the computational time to be decreased from that where the system starts from noise and merely shortens the time taken for the system to leave the linear regime.

TABLE I. Long-pulse–short-wiggler parameters.

N_o	N_e	ρ	$\Delta\bar{z} = 4\pi\rho$	G	S	K
100	400	0.02	0.3	30	$\frac{1}{4}$	1/120

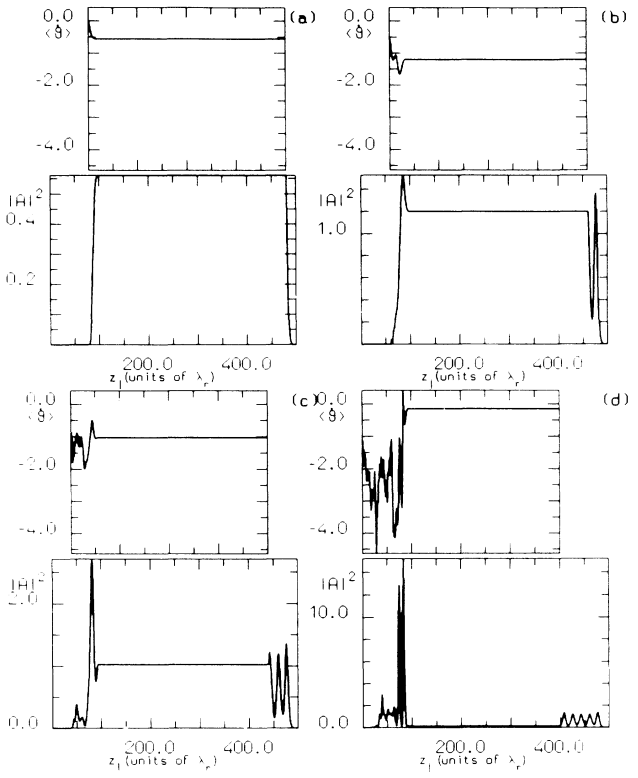

FIG. 1. Long-pulse–short-wiggler case: Radiation and electron pulses after N_P wiggler periods are shown in (a)–(d) for $N_P = 20$, 40, 60, and 100, respectively. $N_0 = 100$, $N_e = 400$, and $G = 30$, giving $S = \frac{1}{4}$ and $K = \frac{1}{120}$.

Evolution in the leading regions of the electron-radiation pulses follows a steady-state behavior with the flat region of the radiation intensity oscillating at the synchrotron frequency; indeed the steady-state evolution of the radiation can be followed as it escapes the leading edge of the electron pulse to propagate in vacuum.

At the trailing edge of the electron pulse there is a region in which the parameters of each electron strip do not evolve identically. This condition occurs because there are no electrons behind and so there is less radiation propagating into this region. The electrons are then radiating practically in vacuum, i.e., spontaneously. This trailing region of the electron pulse can then be considered an intrinsically large slippage region and one in which superradiant behavior may be observable.

The width of this region in the electron pulse after N_P wiggler periods is N_P radiation wavelengths (strips) from the trailing edge, so that the fraction of the electron pulse which has not evolved as the steady state is given by the instantaneous slippage parameter $S_i \equiv N_P/N_e$.

It is seen that radiation emitted from this portion of the electron pulse is quite different in nature from the steady-state evolution. Spikes of high peak intensity are seen to evolve, with peaks many times higher than the steady-state intensity of $|A|^2_{\text{sat}} \simeq 1.4$.[1-3]

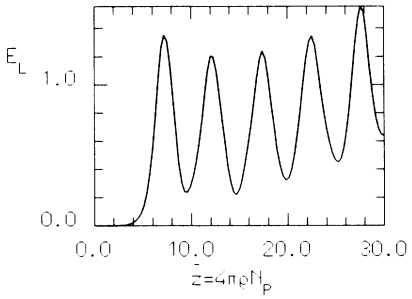

FIG. 2. Long-pulse–short-wiggler case: E_L as a function of dimensionless position, $\bar{z}=(4\pi\rho/\lambda_0)z=4\pi\rho N_P$, through the wiggler.

The pulse evolution in this region is clearly a result of the slippage of the trailing region of the electron pulse and is discussed further in Sec. V and in Ref. 12. The electron or radiation evolution in the steady-state region of the pulses has been reported previously[1–3] and is not considered here further.

A parameter which measures the effectiveness of energy extraction from the electron beam may be defined as

$$E_L=\frac{\mathcal{E}_{\rm tot}-\mathcal{E}_{\rm init}}{N_e}\ , \tag{15}$$

where $\mathcal{E}_{\rm tot}$ and $\mathcal{E}_{\rm init}$ are the total and initial energies, respectively, of the radiation pulse in units of $|A|^2$. This parameter E_L then gives the average energy extracted from the electron pulse in units of $|A|^2$. The efficiency, defined as the ratio between the radiation energy gain and the initial electron energy, is then given by $\eta=\rho E_L$.

As seen in Fig. 2, which plots E_L as a function of the position down the wiggler, E_L oscillates after saturation in a similar way as would be expected from the steady-state theory with maximum $E_L\simeq 1.4$—the spike behavior has little effect in the actual energy extracted from the electron pulse—so that in this sense the steady-state and LPSW models agree.

We now model the LP limit in a long wiggler (LPLW) with the parameters given in Table II. It is seen from Fig. 3 that the effects of slippage are now more dramatic, with the electron pulse slipping a distance greater than its own length L_e. The radiation, however, has already saturated before "escaping" the electron pulse at the leading edge and the spiking behavior of the radiation is clearly seen.

Because the wiggler is long, the spikes may escape from the electron pulse and propagate in vacuum. Unlike the LPSW case, however, where S_i is always <1, once $S_i>1$ there is no flat steady-state region of the radiation pulse.[12]

TABLE II. Long-pulse–long-wiggler parameters.

N_0	N_e	ρ	$\Delta\bar{z}=4\pi\rho$	G	S	K
150	50	0.02	0.24	36	3	1/12

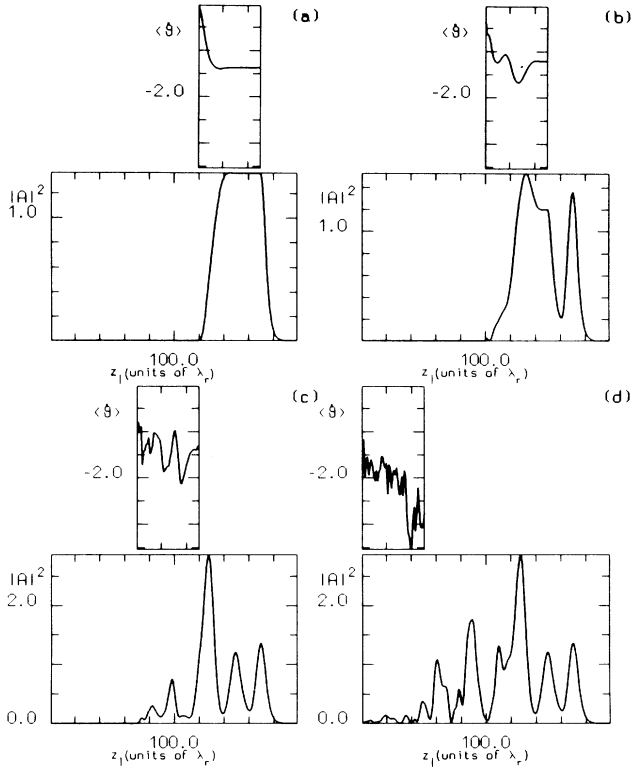

FIG. 3. Long-pulse–long-wiggler case: Radiation and electron pulses after N_P wiggler periods are shown in (a)–(d) for $N_P=30$, 50, 80, and 150, respectively. $N_0=150$, $N_c=50$, and $G=36$, giving $S=3$ and $K=\frac{1}{12}$.

From Fig. 4 we see that E_L may become greater than the steady-state value of $|A|^2_{\rm sat}\simeq 1.4$, the pulse's evolution being determined by the dynamics of the (large) slippage region. Energy extraction is not, however, continuous and tends to a maximum value.

We may conclude that the dynamics of electron or radiation evolution in both the long-pulse regimes are similar—the only difference between the two being the wiggler length.

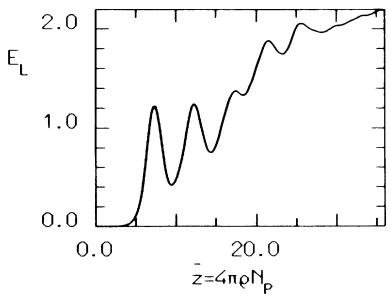

FIG. 4. Long-pulse–long-wiggler case: E_L as a function of dimensionless position, $\bar{z}=(4\pi\rho/\lambda_0)z=4\pi\rho N_P$, through the wiggler.

IV. SHORT-PULSE LIMIT: $K \gtrsim 1$ ($L_e \lesssim L_c$)

We now use the computational model to investigate the high-gain single-pass FEL with short ($L_e \lesssim L_c$) electron pulses. In particular, we wish to investigate the superradiant (SR) regime first predicted in Refs. 8 and 9. Note that there is no high-gain steady-state evolution in the short-pulse limit, since for $G > 1$ and $K \gtrsim 1$, S_i is always greater than 1.[12]

It was suggested[8,9] that radiation emitted by a sufficiently short electron pulse could quickly escape from it—due to the slippage—thereby reducing saturation effects within the pulse.

The escape of emitted radiation has been modeled[8,9] in the steady-state equations by an exponential loss term of the radiation field, proportional to $e^{-K\bar{z}}$, where $\bar{z}$ is the dimensionless distance through the wiggler and the superradiant parameter K is defined in Sec. II. Superradiance was determined to occur when $K \gg 1$. For large values of K it can be shown that the emitted intensity of radiation becomes proportional to n_e^2 instead of the $n_e^{4/3}$ dependence in the steady-state regime. From (7) and (12) we have

$$|A|^2 \propto \frac{|E|_0^2}{\rho n_e}, \quad \rho \propto n_e^{1/3} .$$

The steady-state model predicts a peak field which is independent of ρ ($|A|^2 \propto \rho^0$), so that the emitted radiation intensity $|E_0|^2$ scales as $n_e^{4/3}$; whereas in this dissipative model the assumption $K \gg 1$ leads to a ρ^2 dependence of $|A|^2$, which implies the n_e^2 scaling for the emitted intensity $|E_0|^2$.[8,9]

We note that in the model used here no radiation loss term need be introduced into the equations as the escape of radiation from the electron pulse is included self-consistently. An analytical treatment of the linear evolution of the short-pulse regime, showing this property, is given in Ref. 12.

The same procedure for the representation of both radiation and electron pulses is used as in Sec. III. Again a square, monoenergetic, resonant electron pulse is assumed, and the radiation window is seeded with a field of $|A_0|^2 = 2 \times 10^{-4}$. The parameters used for the series of radiation-electron pulses shown in Fig. 5 are listed in Table III.

TABLE III. Short-pulse parameters.

N_0	N_e	ρ	$\Delta\bar{z} = 4\pi\rho$	G	S	K
100	4	0.02	0.24	24	25	1.01

As with the LPLW case of Sec. III we see the large slippage of the electron pulse with respect to the radiation. Unlike the LPLW, however, the gain of radiation on passing through the electron pulse K^{-1}, is smaller (as $L_e < L_c$) and so there is *no* saturation. The peak intensities of the radiation escaping the electron pulse are then smaller than the steady-state saturation intensity $|A|^2_{\text{sat}}$. No spiking of the radiation is observed as this is only seen to occur after saturation in the LP limit.

In Fig. 6 we show the phase-space evolution of elec-

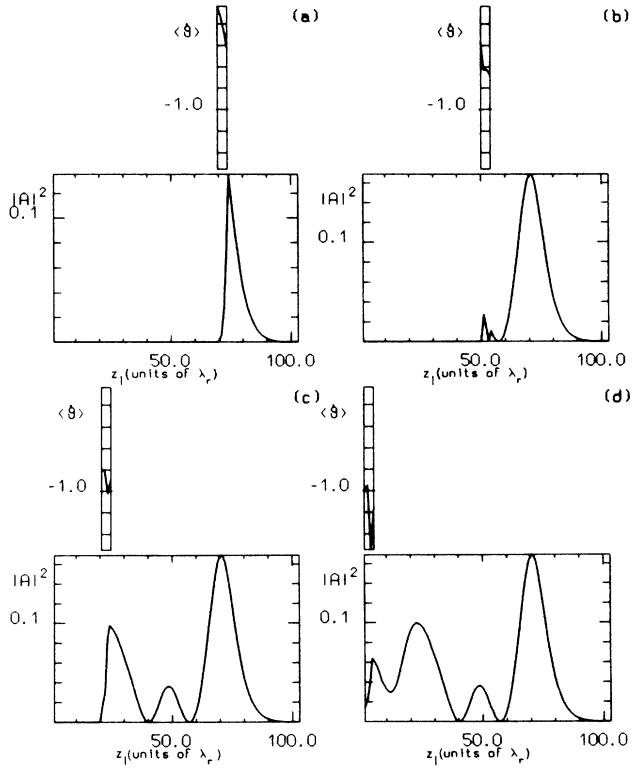

FIG. 5. Short-pulse case: Radiation and electron pulses after N_P wiggler periods are shown in (a)–(d) for $N_P = 30$, 50, 80, and 100, respectively. $N_0 = 100$, $N_e = 4$, and $G = 24$, giving $S = 25$ and $K = 1.01$.

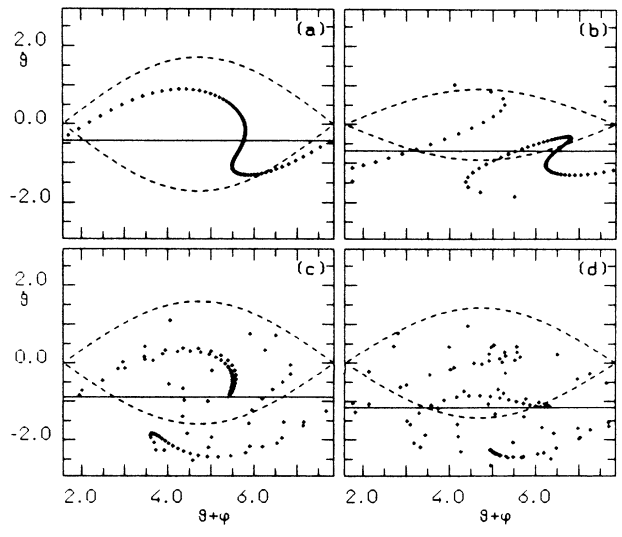

FIG. 6. Short-pulse case: Electrons phase-space evolution in the leading edge of the pulse (position in pulse = 4), at different wiggler positions $N_P = 30$, 50, 80, and 100. The horizontal solid line represents the average electron-energy detuning ($\langle \dot{\theta} \rangle$).

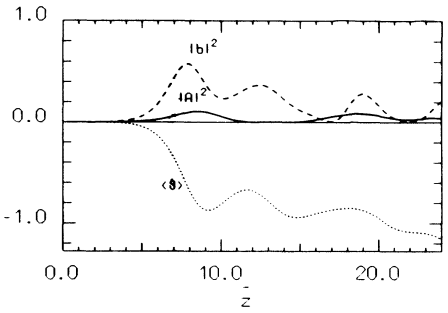

FIG. 7. Short-pulse case: $|A|^2$ (solid line), $|b|^2$ (dashed line), and $\langle\dot{\theta}\rangle$ (dotted line) as a function of position in the wiggler ($\bar{z} \propto N_P$) in the leading electron strip (position in pulse $=4$).

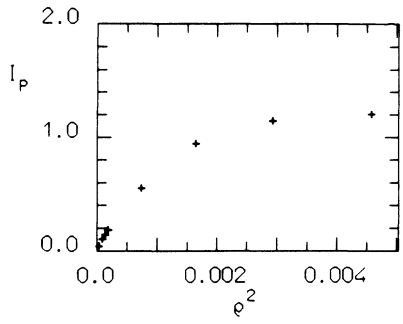

FIG. 9. I_P as a function of ρ^2 for $N_e=6$.

trons in the leading electron strip at various wiggler positions N_P. We include the radiation phase ϕ [so that we are plotting $(\theta_j+\phi,\dot{\theta}_j)$, $j=1,\ldots,N$].

As the intensity of the radiation is smaller than $|A|^2_{\text{sat}}$ the separatrix height $(2\sqrt{2A})$ never becomes greater than the maximum steady-state value of $2\sqrt{2A_{\text{sat}}}$. This is seen from Fig. 6(a), the position $N_P=30$ ($\bar{z}=7.2$), at which the first peak of the intensity escapes the leading edge of the electron pulse. This position also corresponds approximately to the maximum bunching of the electrons in the leading edge, as is seen from Fig. 7. It was derived in Refs. 8 and 9 that for $K\gg1$ (SR regime) the field would evolve as $|A|^2=|b|^2/K^2$. For the parameters here $K=1.01$ and the condition $K\gg1$ does not hold, so that a definite proportionality between $|A|^2$ and $|b|^2$ is not evident.

Because the radiation is continuously escaping due to the slippage, the steady-state conservation law $|A|^2+\langle\dot{\theta}\rangle=$const no longer holds locally within the electron pulse. This feature is seen in the electron phase-space graphs as the electrons escape the separatrix and continue to drop in energy $\langle\dot{\theta}\rangle$ (in the steady state, as electrons lose energy the field increases accordingly, increasing the height of the separatrix, so that the electrons are effectively trapped within the separatrix and eventually reabsorb radiation to perform synchrotron oscillations).

In order to test for superradiance as defined in Refs. 8 and 9 we plot the peak intensity I_P—in units of $|A|^2$—of the *first* pulse of radiation emitted by the electron pulse for various values of ρ^2. [For example, the first pulse of radiation emitted by the electron pulse in Fig. 3 is at position $\simeq 170$, and in Fig. 5 at position $\simeq 70$. This requires a separate run of the computer simulation for each value of ρ^2 (ρ is the only parameter that was changed in the separate runs). Any superradiant emission will then exhibit a linear dependence of I_P on ρ^2 ($|E|^2_0$ is then proportional to the *square* of the electron density n_e).]

In Fig. 8 we preformed six computer runs for six values of ρ^2, with $N_e=3$. These values of ρ^2 correspond to values of K in the range 1.7–5.6. A clear linear dependence is seen, indicating superradiant emission of radiation. We note, however, that the linearity is not perfect with increasing ρ^2 (K^{-1}): as ρ^2 increases the SR behavior diminishes and tends to the LPLW behavior, where I_P has no ρ dependence.

This is seen more clearly in Fig. 9 (where $N_e=6$ and for larger values of ρ^2—corresponding to values of K between 0.20 and 2.4) with I_P tending to "flatten out" to the $|A|^2_{\text{sat}}$ value of about 1.4, completing the transition from the SR to the LP regime. Perhaps the most noticeable difference between the SR and LP regimes is observed when comparing the plots of E_L as a function of the position in the wiggler $\bar{z}$.

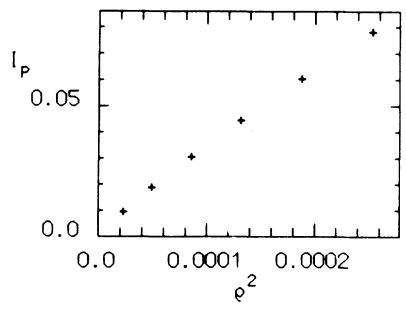

FIG. 8. I_P as a function of ρ^2 for $N_e=3$.

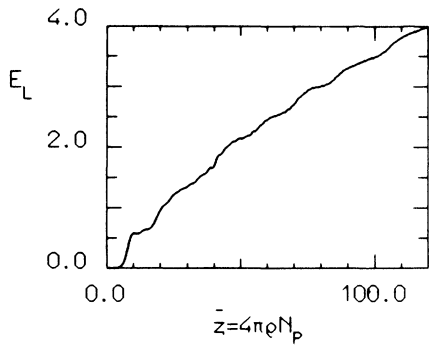

FIG. 10. E_L as a function of $\bar{z}$ in the superradiant regime showing continuous energy extraction from the electron pulse. The same parameters are used as those of Fig. 5, except $N_0=500$.

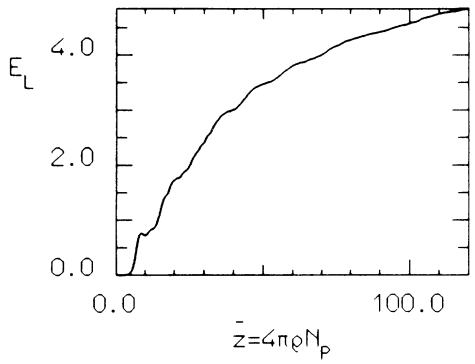

FIG. 11. As in Fig. 10, but doubling the ρ ($4\pi\rho=0.48$) and for $N_0=250$ wiggler periods, giving the same total gain of 120, but a K of 0.55. The E_L no longer exhibits a linear growth, but tends to a saturation value.

Whereas in the LPSW limit the value of E_L never becomes significantly greater than the $|A|^2_{\rm sat}\simeq 1.4$, in the SR regime it is seen (see Fig. 10) that energy is extracted from the electrons at an almost constant rate. This concurs with the phase-space evolution for the electrons. Choosing an adequate undulator length the energy extraction may reach values many times greater than $|A|^2_{\rm sat}$. This is in full agreement with the theory presented in Refs. 8 and 9.

A suitable combination of short-pulse evolution in a waveguide (where slippage may be suppressed[13]) and of tapering of the undulator may overcome this problem and is now under investigation. In the transition region between SR and LPLW, energy extraction can be greater than the steady-state saturation value of 1.4 (see Fig. 11).

V. LONG-PULSE AND SPIKING

It was seen in Sec. III, describing LP evolution, that a previously unreported spiking mode occurs in the slippage region of the radiation pulse. In this section we describe the radiation and the electron evolution in this spiked region.

Since there is no radiation propagating into the trailing edge of an electron pulse, the region one cooperation length L_c from this edge evolves as an independent SR pulse.

We suggest that the electrons entering the slippage region amplify the superradiant pulse emitted by the trailing region of the electron pulse to produce the observed spiking behavior. We call this spiking "*strong superradiance*" to distinguish this case from "*weak superradiance,*" which refers to the short-pulse regime.

In order to test this hypothesis we compare the spiking produced by a long electron pulse system with the SR radiation emitted from the trailing region of the same electron pulse (up to one cooperation length L_c from the trailing edge). From Fig. 12 we see that the position of the spike closely corresponds to the position of the first SR pulse—this correspondence is good for all of a wide range of parameters tested. The peak intensity of the

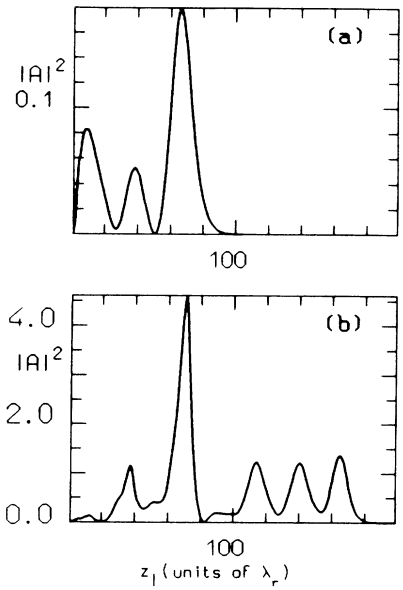

FIG. 12. Amplification of the superradiant pulse emitted by the trailing edge of the electron pulse. The position of the first spike in the slippage region of a long pulse (b) closely corresponds to the position of the first weak superradiant peak emitted by the trailing edge of the same electron pulse (a).

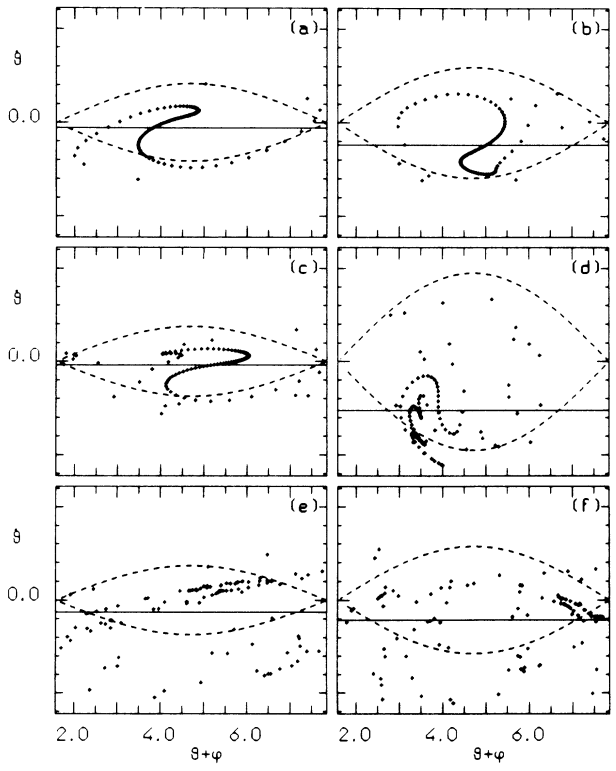

FIG. 13. Long-pulse–short-wiggler case: Electrons phase-space evolution in the leading edge of the pulse at different wiggler positions $N_P=30$, 40, 50, 80, 90, and 100. The horizontal solid line represents the average electron energy detuning ($\langle\dot{\theta}\rangle$).

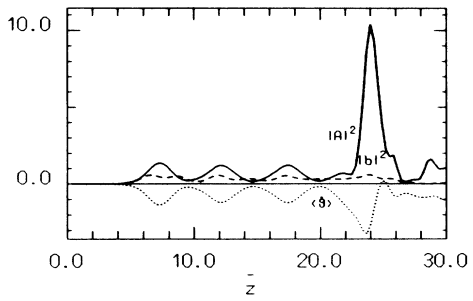

FIG. 14. Long-pulse–short-wiggler case: $|A|^2$ (solid line), $|b|^2$ (dashed line), and $\langle\dot{\theta}\rangle$ (dotted line) as a function of the position in the wiggler ($\bar{z}\propto N_P$) in a fixed position within the electron pulse (in the 60th strip from the trailing edge).

spike (in units of $|A|^2$) has a ρ^2 scaling, which, as seen from the previous sections, indicates a definite SR type process. We now investigate the evolution of the electrons in phase space as they pass through the spike.

The same phase-space representation is used as for the short-pulse evolution of Sec. IV. The evolution of the electrons at position 60 in the electron pulse is shown in Fig. 13 for different wiggler positions N_P. Initially [Figs. 13(a)–(13(c)] the electrons evolve like the steady state, being trapped within the separatrix of maximum height $2\sqrt{2A_{\rm sat}}$ and performing synchrotron oscillations after saturation, so obeying the conservation law $|A|^2+\langle\dot{\theta}\rangle=$const. On entering the slippage region the electrons now interact with the amplified superradiant pulse (i.e., the spike). Because the spike intensity is greater than the steady-state value, the separatrix height increases and the electrons drop in energy ($\langle\dot{\theta}\rangle$) but still remain within the separatrix. This energy drop is seen more clearly in Fig. 14.

Once the electrons have slipped through the spike, however, the separatrix height decreases rapidly and the electrons are no longer trapped. The bunching of the electron has also decreased as seen in Fig. 14.

VI. DISCUSSION

We use the "superradiant parameter," $K=L_c/L_e$, to define the long- and short-pulse regimes in the high-gain single-pass FEL. When $L_e\gg L_c$ ($K\ll 1$), the system operates in the long-pulse regime, and for $L_e\lesssim L_c$ ($K\gtrsim 1$), in the short-pulse regime. We further divide the long-pulse regime into the long-pulse–short-wiggler ($S<1$) and the long-pulse–long-wiggler ($S\gtrsim 1$) limits.

In the short-pulse regime, by computational modeling of the electron-radiation pulses, we have shown the superradiant effect, where the radiation intensity scales as n_e^2 and there are no steady-state-type saturation effects, i.e., energy is continuously extractable from the electrons. We call such radiation in the short-pulse regime weak superradiance.

We observe that previous theories for long electron pulses (steady-state theories) do not fully describe the radiation output from the FEL: there is always a trailing region of the electron pulse in which slippage effects give rise to the previously unreported spiking behavior. We have suggested that a likely mechanism for this spiking could be the amplification of the weak superradiant peak, emitted by the trailing region of the electron pulse, by the electrons entering the slippage region from the steady state. To distinguish this effect from pure superradiance we call this behavior strong superradiance. Although we have not given a fully comprehensive description of the spiking mechanism, work is currently progressing rapidly in this direction.

Throughout the computational results presented here we have always assumed a 1D monoenergetic electron pulse with zero initial detuning ($\partial\theta/\partial\bar{z}_2=0\Longrightarrow\gamma=\gamma_r$), and a square electron-density profile. No detailed studies of the effects of parameters such as the electron-pulse profile, detuning, energy spread, etc., have been performed. We conclude, however, after a preliminary study, that they do not affect the basic underlying mechanism of either the weak or the strong superradiant regimes.

ACKNOWLEDGMENTS

This work was supported by the Istituto Nazionale di Fisica Nucleare (INFN), sezione di Milano. The authors would like to thank the whole Electron Laser Facility for Acceleration (ELFA) group of Milan for helpful conversations and suggestions relating to the work presented her. One of us (B.W.J.M.) was supported by the The Royal Society under the European Science Exchange Programme.

[1]R. Bonifacio, C. Pellegrini, and L. Narducci, Opt. Commun. **50**, 373 (1984).

[2]R. Bonifacio, F. Casagrande, and C. Pellegrini, Opt. Commun. **61**, 55 (1987).

[3]C. Pellegrini and J. Murphy, in *Proceedings of the Joint US-CERN Particle Accelerator School, South Padre Islands, Texas, 1986,* Vol. 296 of *Lecture Notes in Physics,* edited by M. Month and S. Turner (Springer-Verlag, Berlin, 1988).

[4]N. M. Kroll, L. P. Morton, and M. N. Rosenbluth, IEEE J. Quantum Electron. **QE-17**, 1436 (1981).

[5]G. T. Moore, Nucl. Instrum. Methods **A239**, 19 (1985).

[6]T. J. Orzeckowsky, B. R. Anderson, W. M. Fawley, D. Prosnitz, E. T. Scharlemann, S. M. Yarema, D. Hopkins, A. C. Paul, A. M. Sessler, and J. S. Wurtele, Phys. Rev. Lett. **54**, 889 (1985).

[7]W. B. Colson, Nucl. Instrum. Methods **A250**, 168 (1986).

[8]R. Bonifacio and F. Casagrande, Nucl. Instrum. Methods **A239**, 29 (1985).

[9]R. Bonifacio and F. Casagrande, in *Complex System—Operational Approaches,* edited by H. Haken (Springer-Verlag, Berlin, 1985).

[10]See, e.g., *Dissipative Systems in Quantum Optics,* edited by R. Bonifacio (Springer-Verlag, Berlin, 1982).

[11]R. H. Dicke, Phys. Rev. **93**, 99 (1954).

[12]R. Bonifacio, C. Maroli, and N. Piovella, Opt. Commun. **68**, 369 (1988).

[13]R. Bonifacio, L. De Salvo, Nucl. Instrum. Methods **A276**, 394 (1989).